Quaternary Research 78 (2012) 454–464

Contents lists available at SciVerse ScienceDirect

Quaternary Research

journal homepage: www.elsevier.com/locate/yqres

A sedimentary-based history of hurricane strikes on the southern Caribbean coast of Nicaragua

Terrence Allen McCloskey *, Kam-biu Liu

Department of Oceanography and Coastal Sciences, Louisiana State University, USA

ARTICLE INFO

Article history:
Received 24 December 2011
Available online 24 August 2012

Keywords:
Paleotempestology
Hurricanes
North Atlantic
Tropical cyclone hyperactivity
Caribbean
Nicaragua
Paleoecological reconstruction

ABSTRACT

Multi-millennial hurricane landfall records from the western North Atlantic indicate that landfall frequency has varied dramatically over time, punctuated by multi-centennial to millennial scale periods of hyperactivity. We extend the record geographically by presenting a paleostrike record inferred from a four-core transect from a marsh on the Caribbean coast of Nicaragua. Fossil pollen indicates that the site was a highly organic wetland from ~5400–4900 cal yr BP, at which time it became a shallow marine lagoon until ~2800 cal yr BP when it transitioned back into swamp/marsh, freshening over time, with the present fresh-to-brackish *Typha* marsh developing over the very recent past. Hurricane Joan, 1988, is recorded as a distinctive light-colored sand–silt–clay layer across the top of the transect, identifiable by abrupt shifts in color from the dark marsh deposits, increased grain size, and two upward-fining sequences, which are interpreted as representing the storm's traction and suspension loads. The six layers identified as hurricane-generated display temporal clustering, featuring a marked increase in landfall frequency ~800 cal yr BP. This pattern is anti-phase with the activity pattern previously identified from the northern Caribbean and the Atlantic coast of North America, thereby opposing the view that hyperactivity occurs simultaneously across the entire basin.

Introduction

Multi-millennial hurricane landfall records, developed from overwash clastic layers in coastal sediments, have been produced for a number of locations around the western North Atlantic. It has become obvious from these proxy records that landfall frequency has not remained constant over time. Nearly all multi-millennial records have demonstrated relatively abrupt changes in landfall frequency (Liu and Fearn, 1993, 2000; Scott et al., 2003; Liu, 2004; Donnelly and Woodruff, 2007; Scileppi and Donnelly, 2007; Mann et al., 2009, McCloskey and Keller, 2009), with landfall increasing as much as five-fold during active periods (Liu, 2004). The duration of individual activity regimes is typically on the order of several hundred to >2000 yr. Correlating hyperactive periods with known paleoclimatic conditions should prove useful in identifying the climatic/atmospheric features driving these changes. Current discussion is focused on the timing of these activity regime shifts. One model suggests that regime changes occur simultaneously across the entire North Atlantic basin with increased activity corresponding to La Niña-like conditions and high Atlantic sea surface temperatures (SST) (Mann et al., 2009). The second model argues that the hyperactivity is time-transgressive, with a band of maximum hurricane activity migrating latitudinally across the North Atlantic (Liu and Fearn, 2000; Liu, 2004). In the latter, the main driver is the pole-equator temperature gradient, with cold periods forcing hurricane activity to the south, and warm periods forcing activity to the north (McCloskey and Knowles, 2009). Increasing the number and spatial distribution of long-term landfall records should help resolve this question. Here we present a proxy record from the southern Caribbean coast of Nicaragua near the southernmost fringe of Atlantic hurricane landfalls (Fig. 1b).

Geographical setting and study site

The Caribbean coast of Nicaragua (Fig. 1b) is a wide (up to 150 km), low-gradient coastal plain sitting atop a deep, tectonically stable sedimentary basin composed of material that has been eroding from the highlands to the west since the Triassic (Mills and Hugh, 1974; Marshall, 2007). Erosion continues at a high rate; approximately 15 times more sediment per unit length is delivered annually to the Caribbean coast of Nicaragua than the Atlantic coast of the United States (Roberts and Murray, 1983). The plain is covered by a pine savannah crossed by sediment-laden rivers, while the coast is dominated by wetlands, especially mangrove swamps and tidal lagoons, behind sandy beaches (Parsons, 1955; Wallace, 1997; Christie, 2000; Marshall, 2007). The area has a tropical wet climate; mean annual temperature is 26°C, and annual rainfall can exceed 500 cm (Christie, 2000; Marshall, 2007), mainly falling during the wet season from June through January. Evaporation can exceed precipitation during the dry season from February through May (Brenes et al., 2007).

* Corresponding author at: Department of Oceanography and Coastal Sciences, 3251 Energy Coast and Environment Building, Louisiana State University, Baton Rouge, LA 70803, USA. Fax: +1 225 578 6423.
E-mail address: tmcclo1@tigers.lsu.edu (T.A. McCloskey).

0033-5894/$ – see front matter © 2012 University of Washington. Published by Elsevier Inc. All rights reserved.
doi:10.1016/j.yqres.2012.07.003

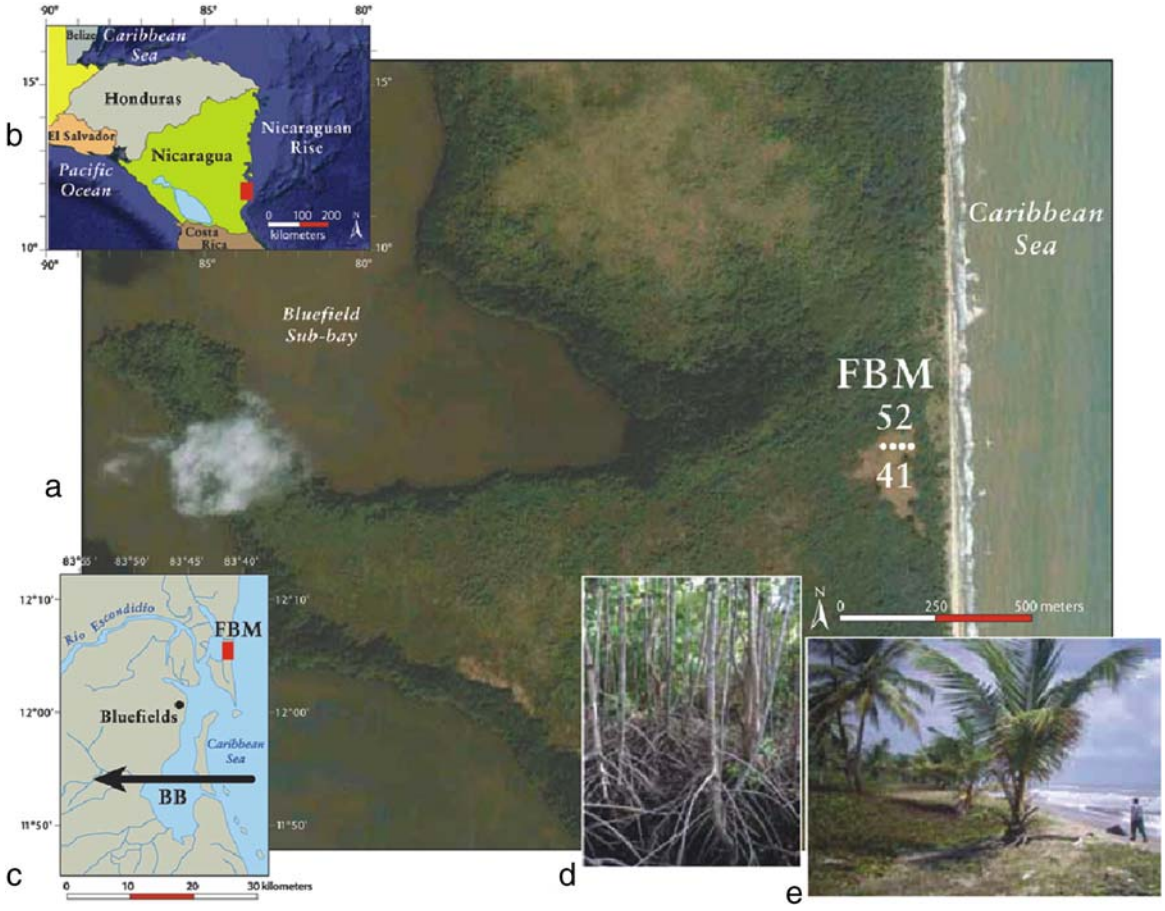

Figure 1. Location of study site. The coring site is located on the Caribbean coast of Nicaragua in the area covered by the red box in (b), which corresponds to the larger-scale map of Bluefields Bay (c). The black arrow represents the path of Hurricane Joan in 1988, and the red box indicates the coring site, depicted in greater detail on the GoogleEarth image (a), which displays the spacing and location of the four cores extracted from Falso Bluff Marsh (FBM). The Caribbean shoreline (e) is covered by an open-canopy palm grove behind a sandy beach, whereas the muddy, low energy sub-bay to the west is fringed by a dense red mangrove forest (d).

Bluefields Bay (BB), located along the southern end of the microtidal (tidal range: 22 cm) coast (Fig. 1c), is a large, shallow, turbid, low-energy estuarine lagoon, fed by four rivers (Brenes et al., 2007). The estimated annual discharge and sediment load of the largest, Rio Escondido, are $>26\times10^9$ m^3, and $>4\times10^6$ m^3, respectively (Roberts and Murray, 1983). A large island blocks the eastern entrance of the bay, restricting connection to the sea to narrow channels at its north and south ends. Our coring site, Falso Bluff Marsh (FBM) (Fig. 1a), is situated at 12°6.72′N, 83°41.42′W, along the eastern edge of a low, forested peninsula separating the bay from the Caribbean. The Caribbean side, an exposed coast, is dominated by clear water, sandy beaches, and open-canopy coconut and palm groves above a grassy ground cover (Fig. 1e). The sub-bay to the west is a muddy, low-energy system, dominated by a thick fringe of red mangroves (*Rhizophora mangle*) at the water edge and tropical forest at the slightly higher land inland (Fig. 1d). The peninsula is at least 750 m wide near FBM. Cores were extracted from a cattail (*Typha*) marsh filling a small depression beginning ~100 m inland from the Caribbean behind a berm ~1.5 m in height.

Hurricane Joan, a category 4 hurricane with maximum sustained wind speed of 232 kph (144 mph) crossed the southern part of Bluefields Bay in October 1988 (Fig. 1c). It devastated the town of Bluefields and the surrounding area, causing severe damage to >500,000 ha of tropical forest (Lawrence and Gross, 1989; Boucher, 1990; Vandermeer et al., 2000). Rainfall was heavy, causing "raging" floods that destroyed >30 bridges and washed out >644 km (>400 miles) of roads (Gerrish, 1989).

Methods

Four cores were extracted from the FBM at distances of 100, 120, 132, and 156 m from the sea. Both a Russian peat borer and a modified Livingstone piston corer were used to obtain the four sediment cores. The peat borer cores were extracted in 50 cm sections with minimum overlaps of 5 cm; piston cores section lengths varied from 75 to 138 cm with at least 8 cm overlap. Extraction was through a sequence of cores in slightly offset holes until refusal. All cores were photographed in the field. All coring and sampling locations, as well as position of beach berms and high and low tide lines were determined by a handheld GPS unit. Cores were sealed in the field before being transported to Louisiana State University. When opened the cores were photographed and the composition, structure, color and stratigraphy described. Loss-on-ignition (LOI) analysis was conducted continuously at 1 cm resolution (Dean, 1974) to determine water, organic, carbonate, and residual percentages. In order to shed light on the depositional mechanism and origin of the clastic layers, 1 cm^3 samples, taken at 1 cm intervals from within the top clastic layer in each core, were sent to Memorial University in St. John's, Newfoundland for grain size analysis by means of a Horiba LA-950 laser particle size analyzer.

Pollen was processed using the procedure described by Faegri and Iverson (1989) and counted and identified at approximately 10 cm intervals throughout the core. Except in a few samples with low pollen concentrations, a minimum of 300 grains were counted per sample. Two sediment samples were examined cursorily for diatoms.

https://doi.org/10.1016/j.yqres.2012.07.003 Published online by Cambridge University Press

Small quantities of plant detritus were separated from the surrounding matrix in distilled water, handpicked under a microscope and sent to the National Ocean Sciences AMS (NOSAMS) Facility at Woods Hole Oceanographic Institution for radiocarbon dating (Table 1). Dates were calibrated to 'calendar' years with the Calib 6.0 program (http://calib.qub.ac.uk/calib/calib.html), using the Reimer et al. (2009) dataset. Age–depth models were developed for each core based on the "best-fit" regression line for the calibrated dates. For samples which calibrated (at 2σ) to a single calendar date range the selected date was the range's midpoint, for samples calibrated to two or more date ranges, the calendar date was calculated by multiplying each range's midpoint by probability of occurrence for the range and then summing for each sample.

Results

Core FBM1

FBM1 is the longest of the cores, and the most seaward, located 100 m inland. It consists of eleven 50 cm Russian peat borer sections, reaching a depth of 489 cm. This core can be divided into four lithologic zones, based on the LOI results (Fig. 2).

Zone 4 (489–436 cm) is basically a highly decomposed black peat, with both water and organic percentages near 85%. The few minor drops in these levels (organic drops to 70% at 464 cm) do not present visually. The transition to Zone 3 shows a few small fluctuations in composition and water and organic percentages.

Zone 3 (435–251 cm) is almost entirely a featureless, unlaminated gray clay. Apart from the narrow peat band centered at 390 cm, water and organic contents remain consistent throughout the zone, ~55% and 15%, respectively. The peat band is 3 cm thick, and contains some larger organic pieces. A sample from 336 cm contains 13 exclusively marine diatom species (Luo Wang, personal communication, 2010).

Zone 2 (250–95 cm) consists of a decomposed black peat above 190 cm, with water and organic values consistently >80% and >70%, respectively. Two clastic bands occur; a brownish-gray clay band at 198–206 cm and F, a brown clay band at 137–144 cm, both marked by sharp drops in organic percentages. Below 190 cm the peat becomes increasingly less organic and lighter colored, changing to muddy peat at ~230 cm and peaty clay at ~240 cm. Below 250 cm the water content drops below 60%.

Zone 1 (1–94 cm) is generally peat and/or muddy peat, interrupted by mineral (sand/silt/clay) bands with very high residual percentages. Above 60 cm, the organic intervals generally consist of a brownish peat, containing some large, partially decomposed organic material, often recognizable as individual leaves or roots. Water content varies between 58 and 73%, and organic contents between 24 and 69%. Below 60 cm the organic material becomes darker and more decomposed, with higher water (>70%) and organic (>50%) content. Five distinct clastic layers (A–E) occur in this zone, at 5–6, 40, 45–57, 66–68, and 80–94 cm. Layer A fines upward from a base of orange–white medium sand to a darker, more organic clay at the top, with minimum water and organic content of 12.5% and 2.5%, respectively. Layer C is very similar in thickness, water/organic values, composition and structure, similarly fining upward from orange–white sand to darker organic clay. Layers B, D and E are composed of clay, with minimum water and organic values of ~50 and >20%, respectively. A sample from the surface (1 cm) contained 18 fresh-to-brackish species of diatoms (Luo Wang, personal communication, 2010).

Pollen

The pollen diagram (Fig. 3) shows the same four zones, although the vegetation transition from Zone 3 to Zone 2 lags behind the lithologic change. The zonation is based principally on the relationship between *Ilex*/*Myrica* and *Rhizophora* (red mangroves), with *Ilex* and *Myrica* increasing/decreasing in tandem, anti-phase with *Rhizophora*. Zone 4 shows high *Ilex* and *Myrica* and low *Rhizophora* levels. In Zone 3, *Rhizophora* levels rise steadily, while *Ilex* and *Myrica* drop. This trend reverses in Zone 2, with *Rhizophora* decreasing while *Ilex* and *Myrica* increase, along with the appearance of Palmae, which reaches a peak of >65% at 151 cm. In Zone 1 the trend again reverses with *Ilex* and *Myrica* decreasing and *Rhizophora* increasing until ~70 cm, after which *Rhizophora* percentages decrease while various forest taxa (Leguminosae, Sapotaceae, Euphorbiaceae, Bignoniaceae, and Palmae) increase. Around 30 cm Cyperaceae and Polypodiaceae increase, with *Typha* spiking to >65% at 8 cm.

Chronology

The results for the four dated samples are listed in Table 1 and shown stratigraphically in Figure 2. The age–depth model is cal yr BP = 11.4 * Depth (cm) − 182, producing a calculated sedimentation rate of 0.09 cm/yr and an intercept (surface date) of −182 years. The intercept date can be explained by postulating a slightly higher sedimentation (0.10 cm/yr) rate above the topmost date, which may be due to less compaction in the upper part of the core (Fig. 4). The 346 cm gap between the two deepest sampling depths likely masks sedimentation rate changes accompanying the changes in depositional material (peat–clay–peat).

Core FBM2

FBM2, located 120 m from the sea, 20 m inland from FBM1 (Fig. 5), consists of three Russian peat borer sections with a total depth of 126 cm. This core is generally peat, interrupted by five distinct clastic layers (A–E) at 5–14, 41–44, 54–63, 74–75, and 98–110 cm. Layer A fines upwards from a gray sand through a brown silt to clay with minimum water and organic values of 26% and 3%, respectively. Layer C is

Table 1
Radiocarbon results for cores FBM1, 4, and 5.

Lab #	Core	Depth (cm)	Age ^{14}C yr BP	Age (2σ) cal yr BP	Probability	Age (2σ) AD/BC	δ^{13}C (‰)	Material
OS-70924	FBM1	61	495 ± 50	465–564	0.845	1386–1485 AD	−29.69	Plant/wood
				589–641	0.155	1309–1361 AD		
OS-70861	FBM1	70	775 ± 25	673–731	1.000	1219–1277 AD	−29.54	Plant/wood
OS-70926	FBM1	98	885 ± 35	730–910	1.000	1040–1220 AD	−27.33	Plant/wood
OS-70862	FBM1	444	4310 ± 30	4835–4893	0.767	2944–2886 BC	−28.15	Plant/wood
				4897–4960	0.233	3011–2948 BC		
OS-72533	FBM4	139	850 ± 30	689–797	0.940	1153–1261 AD	−27.39	Plant/wood
				818–821	0.004	1129–1132 AD		
				870–898	0.056	1052–1080 AD		
OS-70707	FBM5	56	875 ± 30	726–832	0.762	1118–1224 AD	−29.07	Plant/wood
				845–907	0.238	1043–1105 AD		
OS-73423	FBM5	189	2650 ± 35	2736–2812	0.904	863–787 BC	−29.9	Plant/wood
				2816–2844	0.096	895–867 BC		

https://doi.org/10.1016/j.yqres.2012.07.003 Published online by Cambridge University Press

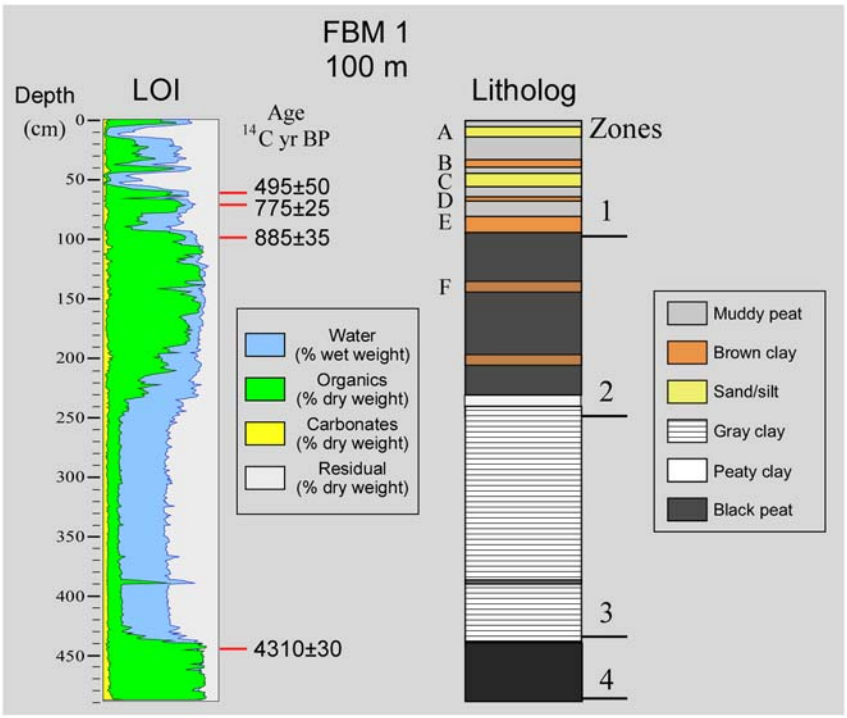

Figure 2. Loss-on-ignition curve (left) and litholog (right) of core FBM1. Radiocarbon dates are shown in their stratigraphic position on the left, with the sedimentary zonation scheme depicted in the center and prominent sedimentary layers on the right.

similar, fining upward from sand to clay. Layers B, D and E are composed of clay with minimum water and organic values of 53–70% and 10–28%. There is a rather indistinct brown clay layer at 93–94 cm with much higher water and organic values. The peat matrix is characterized by high organic and water contents, low carbonates (peaking <8.5%, and usually <5%). Overall, FBM2 closely resembles Zone 1 of FBM1.

Core FBM4

FBM4, located 132 m from the sea, 12 m inland from FBM2, is a composite core 194 cm long, consisting of two piston corer sections with a 13 cm overlap. This core is predominately peat, interbedded by distinct clastic layers at 5–13, 22–28, 32–38, 50–53 cm (A–D), 60–100 cm, 141–143 cm (E), and 174–76 cm (F) (Fig. 5). Below 108 cm the water and organic contents increase for the peat, at times exceeding 85 and 70%, respectively. Layers A, B, and C plus the interval from 60 to 100 cm all contain sand, while layers D, E and F consist of silt and/or clay. The interval from 60 to 100 cm is physically different from the other clastic layers in the transect, consisting of a structureless mix of sand, pebbles and organics, including extremely large wood fragments at top and bottom. A single sample of plant material, extracted from 139 cm, produced a radiocarbon date of 850±30 ^{14}C yr BP (Fig. 5). This calibrates to three date ranges from 689 to 898 cal yr BP (Table 1, Fig. 4).

Core FBM5

FBM5, collected at 156 m from the ocean, is the most landward core, 24 m inland of FBM4. The two overlapping piston sections penetrated to 256 cm with an 8 cm overlap. The topmost section (to 71 cm) resembles Zone 1 of core FBM1 consisting of a peat matrix (water generally >80%, organic ~70%) interrupted by five clastic layers (A–E) at 3–6, 24–25, 28–39, 46–47 and 58–70 cm. Layers A and C contain sand fining to clay, with C having minimum water and organic content of 27% and 2.5%. Layers B, D and E are brown clay. The interval from 72 to 192 cm is very similar to Zone 2 in FBM1, composed of peat with a brown clay layer (F) at 121–22 cm. The section from 177 to 192 cm is slightly less organic and contains two barely visible gray clay layers at 174–175 cm and 178–181 cm. The material below 192 cm is a massive gray clay, resembling the material in Zone 3 in FBM1 in color and texture and having similar water, organic and residual values (Fig. 2). The date from the sample from

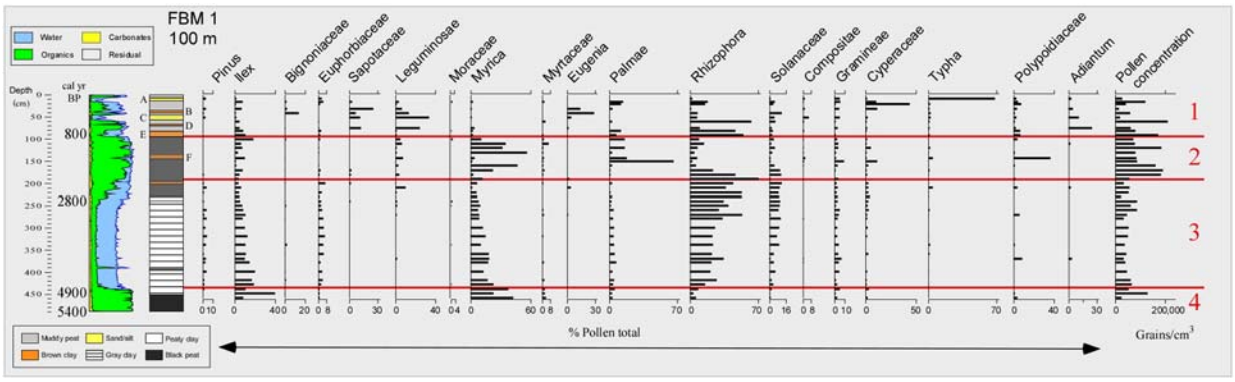

Figure 3. LOI curve, litholog and pollen diagram for core FBM1. Palynological zones are marked on the right.

https://doi.org/10.1016/j.yqres.2012.07.003 Published online by Cambridge University Press

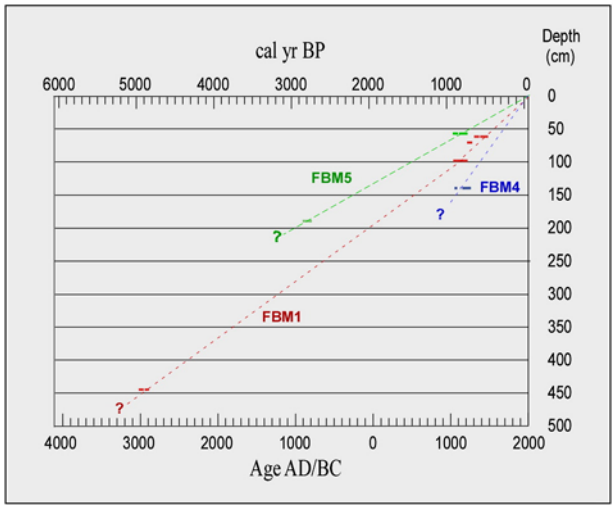

Figure 4. Age–depth graph for cores FBM1, FBM4 and FBM5. 'Calendar' ages calibrated from the radiocarbon dates (2σ) are plotted for the seven dated samples.

56 cm (875 ± 30 ^{14}C yr BP; 726–907 cal yr BP) overlaps with dates from FBM1 and 4. The sample from 189 cm was dated to 2650 ± 35 ^{14}Cyr BP (2736–2844 cal yr BP) (Fig. 5).

Grain size characteristics

Mean, median and mode grain sizes and sand/mud ratios all decrease upcore in the top clastic layer in cores FBM2, 4, and 5 (Table 2). The upward fining occurs in two sequences corresponding to two stratigraphic units, a sand layer at the bottom and a sand/silt/clay layer on top. Both units fine upward, with the bottom of the top unit at times having slightly larger grain characteristics than the top of the bottom unit, as measured by both grain size and sand/mud ratios in FBM4. The layer thins landward with grain size decreasing across both the bottom and top of the layer.

Sediment samples collected from the beach in front of FBM and from the bottom of the sub-bay immediately to the west display markedly different grain size characteristics. A sample collected from the beach was 100% sand, while >80% of a sample collected from the bottom of the sub-bay was silt or clay. Mean, median and mode grain sizes were all at least an order of magnitude larger for the beach material (Table 2). The LOI data show distinct compositional differences between the two source areas as well, with the bay sample containing much higher percentages of water (43 vs. 7%), organics (12 vs. 0.5%) and carbonates (7 vs. 0.5%), and a corresponding decrease in residual material (81 vs. 99%) (Table 3).

Discussion

Stratigraphic correlation of cores along transect

The stratigraphic zones described for FBM1 can be extended across the transect (Fig. 5). Zones 1 and 2, encountered in all cores, are both characterized by dark organic material with high organic and water percentages, except where interrupted by the clastic layers. Zone 2 is distinguished from Zone 1 by the reduced frequency of these clastic layers. Zone 3, encountered in FBM1 and 5, consists of gray clay with low water and organic percentages. Zone 4, encountered only in FBM1, consists of a dark organic material with high water and organic contents.

The close stratigraphic correlation between the cores, especially FBM1 and FBM5, permits a composite dating scheme for all zone boundaries, based on the dating of plant detritus at the zone boundaries. The bottom of Zone 1 was dated from three cores, producing overlapping dates of 850 ± 30 ^{14}C yr BP, 875 ± 30 ^{14}C yr BP and 885 ± 35 ^{14}C yr BP, which calibrate to six dates ranges from 689 to 910 cal yr BP. The bottom of Zone 2 in FBM5 is dated at 2650 ± 35 ^{14}C yr BP (2736–2844 cal yr BP), while the bottom of Zone 3 (444 cm, FBM1), is dated to 4310 ± 30 ^{14}C yr BP (4835–4960 cal yr BP). The calibrated calendar ages for the zone

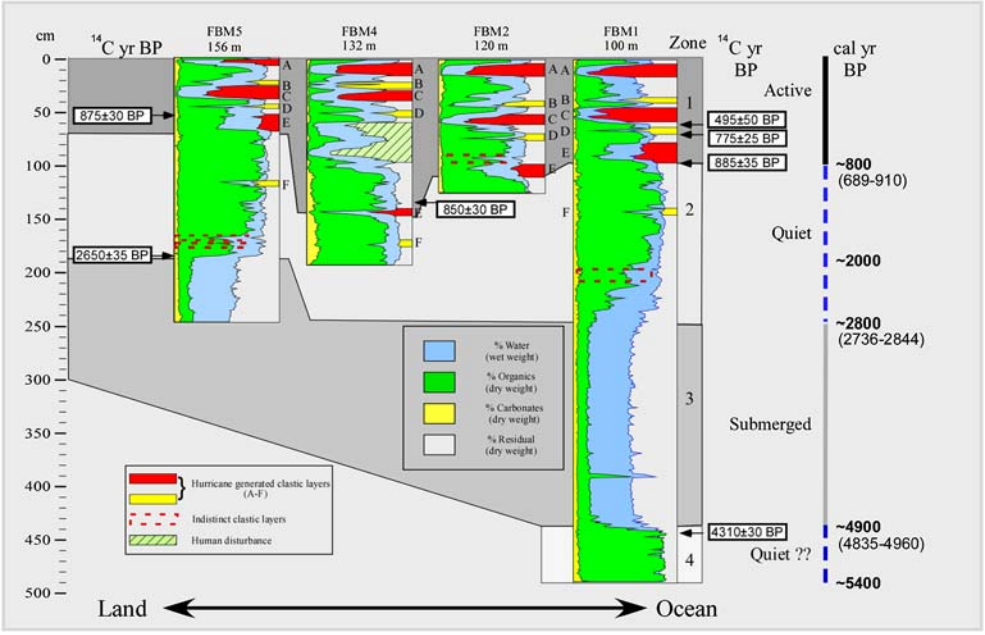

Figure 5. LOI curves for the four-core transect, detailing the percent water, organics, carbonates, and residual. Four zones are recognized, based on the sedimentary profile. Hurricane-generated clastic layers (A–F) are indicated by red and yellow shaded boxes for visual clarity, color of shading has no significance. The clastic interval marked by the green hatched box in FBM4 that does not correspond to similar layers across the transect probably results from human disturbance. Radiocarbon dates and error bars for seven organic samples are shown. The approximate calendar dates for the zone transitions, rounded to the nearest century, are shown on the far right, with the possible 2σ date ranges listed below in parentheses. The vertical bar indicates inferred tropical cyclone activity regimes, with periods marked as "Active," "Quiet" or "Submerged."

https://doi.org/10.1016/j.yqres.2012.07.003 Published online by Cambridge University Press

Table 2
Grain-size characteristics of clastic layer A in cores FBM2, 4, and 5 and surface samples from the bay and beach near FBM.

	cm	Mode (μm)	Mean (μm)	Median (μm)	Sand/mud ratio
FBM2	5–6	50.6	42.8	39.5	0.3
	6–7	50.8	44.8	41.0	0.3
	7–8	51.0	45.0	40.1	0.3
	8–9	58.1	53.9	51.0	0.5
	9–10	58.2	54.9	53.2	0.5
	10–11	58.5	57.0	55.4	0.6
	11–12	76.0	72.5	68.7	1.5
	12–13	76.6	76.8	72.3	1.8
	13–14	88.7	104.2	93.1	2.7
FBM4	5–6	51.0	43.6	46.1	0.3
	6–7	67.0	61.0	64.0	0.9
	7–8	76.0	67.1	70.6	1.3
	8–9	76.4	70.9	74.9	1.7
	9–10	67.5	64.0	65.2	1.1
	10–11	76.3	74.1	78.4	2.2
	11–12	77.5	79.8	87.4	2.7
	12–13	87.8	89.7	108.0	2.9
FBM5	3–4	44.4	39.4	31.8	0.2
	4–5	58.7	59.9	56.6	0.7
	5–6	58.7	55.0	53.4	0.6
Bay		19.1	36.3	21.4	0.2
Beach		311.1	360.3	334.8	Infinity

Table 3
Compositional characteristics of the top and bottom cms of clastic layer A in cores FBM2, 4, and 5 and surface samples from the bay and beach near FBM.

	cm	%Water	%Organic	%Carbonates	%Residual
Top-layer A					
FBM2	5–6	55.28	12.08	1.61	86.31
FBM4	5–6	66.76	14.53	2.43	83.04
FBM5	3–4	47.00	7.67	2.16	90.16
Bay		42.67	12.22	6.96	80.82
Bottom-layer A					
FBM2	13–14	25.76	3.01	1.37	95.62
FBM4	12–13	27.28	3.62	1.02	95.36
FBM5	5–6	43.14	6.85	1.79	91.36
Beach		7.02	0.46	0.41	99.12

boundaries, rounded off to the nearest century, are listed in bold type on the extreme right of Fig. 5, with the 2σ date ranges shown below in parentheses. The age of the initiation of deposition at FBM 1, calculated from the age–depth model, is ~5400 cal yr BP, with an uncertainty of ~200 yr, as inferred from the age uncertainty in the rest of the core.

Reconstruction of environmental history

Sedimentary, pollen, and diatom evidence from FBM1 shows that the depositional environment did not remain constant at this location since ~5400 cal yr BP. The earliest environment (Zone 4), beginning ~5400 cal yr BP, most likely represents a backbarrier swamp, surrounded by bushes and tropical forests (Fig. 6). Zone 3, beginning ~4900 cal yr BP, shows a sudden shift from organic to mineral deposition and an apparent steady upcore rise in salinity, as suggested by *Rhizophora* pollen reaching 70% at the top of the zone. The low pollen concentration levels, featureless gray clay lacking *in situ* plant roots, and the exclusively marine diatoms suggest that this zone represents a shallow low-energy marine lagoon behind a partially submerged sand barrier, with *Rhizophora* dominating the tidal mudflats and forming a fringing forest on the supratidal areas (Fig. 6). At the beginning of Zone 2, ~2800 cal yr BP, salinity drops markedly as mangroves are replaced by less halophytic species such as *Myrica* and palms, probably representing the development of a backbarrier swamp, very similar to that existing during Zone 4. This continues until ~800 cal yr BP (Zone 1) at which time mangroves apparently experience a brief resurgence, although the spikes in *Rhizophora* pollen possibly represent episodes of waterborne pollen transport from the back bay during extreme events and not an actual increase in mangrove populations at the site (see below). This is followed by an increase in tropical forest species (e.g., Sapotaceae, Leguminosae, Myrtaceae) and a marsh dominated by sedges and cattails (*Typha*), indicating progressive freshening and increasing terrestrial site characteristics throughout the recent centuries. The present marsh is very young, with *Typha* pollen practically nonexistent below 8 cm.

The marine conditions in Zone 3 probably results from sea-level rise. Assuming that core tops are at approximately present sea level, FBM1's basal depth (489 cm) puts it slightly above the estimated sea level (~5 m below present) for 5400 cal year BP (Toscano and Macintyre, 2003). By 4900 cal year BP, the beginning of Zone 3, sea level was only ~4 m below present, while the sediments were 444 cm below present surface level. Sudden flooding related to sea level rise and the overtopping of the beach barrier could be expected in this case, capable of abruptly turning a fresh-to-brackish swamp into a marine lagoon with an environment much like the current sub-bay to the west, favoring the development of mangroves along the shorelines. By the end of Zone 3 at ~2800 cal yr BP, deposition (189 cm depth at FBM5) had caught up with sea level, estimated at ~2 m below present (Toscano and Macintyre, 2003).

Sedimentology of clastic layers

The clastic layers share several common features that clearly distinguish them from the organic matrix in which they are embedded, including sharp bottom contacts, increased grain size, increased mineral content, and lighter color. Individual clastic layers can be correlated across the transect based on a combination of stratigraphic correspondence and distinguishing sedimentary features, i.e. layer thickness, grain size, composition, and color. Radiocarbon dating supports this cross-correlation, as samples from the top of Layer E from FBM5 and FBM4 and the bottom of the layer from FBM1 produced overlapping radiocarbon dates, indicating that layer E has statistically identical ages across the transect.

The clastic layers can be divided into three sedimentary types:

Type 1—sand–silt–clay

Layer A thins inland, decreasing in thickness from 10 cm at FBM1 and 2 (100 and 120 m from the sea, respectively) to ~8 cm at FBM4 (132 m), to ~5 cm at FBM5 (156 m). Grain-size analysis conducted on cores FBM2, 4, and 5 demonstrates that this layer fines both inland and upward in each core, divided into two distinct stratigraphic units. This same pattern is visually obvious in FBM1, although not enough material remained after sampling for other analyses to perform quantitative grain-size analysis (Fig. 7, Table 2).

Layer C is very similar. The material in all four cores fines from sand to clay, with the two seaward cores (FBM1, 2) capped by a mud drape, while the two landward cores (FBM4, 5) are dominated by gray clay above a thin sand base. Except for an especially thick layer in FBM5, landward thinning and layer thickness for individual cores achieve a very close match with layer A.

Type 2—brown clay

Layers B, D, E and F are generally smaller grained and thinner than layers A and C, composed of distinct horizontal bands of brown clay with sharp bottom contacts. Sand grains and gray clay occur only in layer B at FBM4. The indistinct clastic layers occurring near the bottom of Zone 2 (dashed lines, Fig. 5) differ from the other type 2 layers. The layer at ~200 cm in FBM1 does not present as a distinct

https://doi.org/10.1016/j.yqres.2012.07.003 Published online by Cambridge University Press

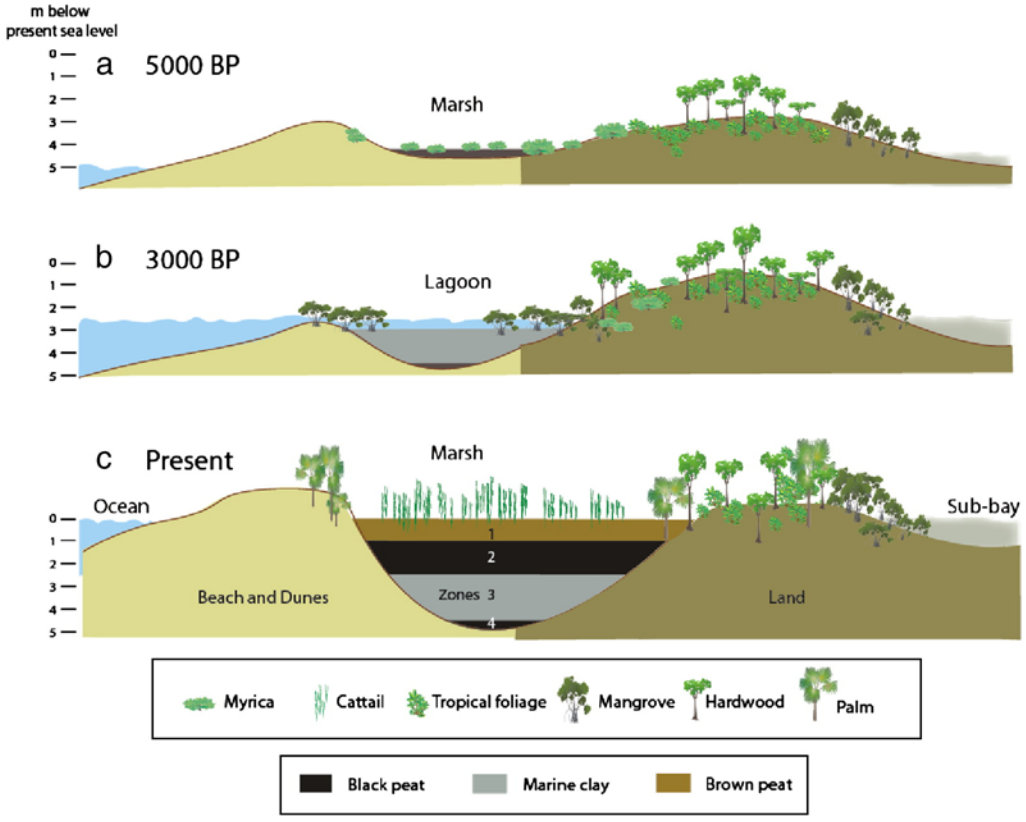

Figure 6. Inferred paleoenvironmental conditions. 5000 yr ago (a) the site was probably a backbarrier swamp, surrounded by bushes and tropical forests, slightly above sea level, with mangroves forming a thick fringe along the sub-bay to the west. 3000 yr ago (b) the site was a shallow marine lagoon, dominated by mangroves. Presently (c) the site is a dense *Typha* (cattail) marsh with tropical hardwoods present in the surrounding forest. Mangroves again form a thick fringe along the sub-bay to the west. Deposition was a gray marine clay 3000 yr and peat at 5000 yr ago and at present.

horizontal unit, but rather as brownish sections of clayey peat scattered throughout an 8 cm peat interval. The two layers occurring from 160 to 180 cm in FBM 5 are even less distinct and, unlike other type 2 layers, composed of gray clay resembling the material in Zone 3.

Type 3—structureless

The clastic layer occurring at 60–100 cm in FBM4 is a chaotic mix of mineral and organic materials of various sizes.

Origin of clastic layers

It is unlikely the clastic layers result from "normal" (non-event) deposition, which is dominated by autochthonous organic production throughout zones 1 and 2. The time intervals associated with these layers appear to be too short and the changes too abrupt to result from changes in the environmental boundary conditions. Investigating the origin of the clastic material offers a possible method of identifying their proximate cause.

Type 1—bimodal

The first clastic layer type, which occurs in layers A and C, displays two normally-graded stratigraphic units, fining from sand to clay. Possible sources of this material are the Caribbean Sea to the east and Bluefields Bay to the west. Sediments from the two source areas can be readily distinguished as the bay sediments are much finer-grained and more organic. The top stratigraphic unit in layer A resembles the bay material, while the bottom unit, being coarser and more mineral-rich, is a better match with the beach sediments (Tables 2 and 3). This suggests that the material at the bottom of the layer originated from the beach and near shore to the east, while the top material either originated in the Bluefields Bay to the west or is derived from the same sources as the bay material.

The most likely explanation for the sedimentary signature of layer A is an intense hurricane, with the lower stratigraphic unit representing the traction load deposited by storm surge and the upper unit representing the settling of the suspension load. The lower unit, a distinct sand layer with sharp bottom contacts that fines upward and landward and thins landward matches the well-recognized sedimentary profile of overwash fans (Donnelly and Webb, 2004; Liu, 2004; Williams, 2009, 2010). That the mean grain size in layer A is smaller than that of the beach sample merely indicates that the largest beach material was either too large to be transported or dropped out before reaching the marsh. The upper stratigraphic unit is a smaller-grained drape that fines from sand to clay, matching the profile of material identified as suspension loads deposited by hurricanes along the northern Gulf Coast (Williams, 2009, 2010). At FBM a hurricane-generated suspended load could be delivered either from the ocean directly by storm surge or from the back bay as a result of flooding. Storm surge can dramatically raise the water level inside the small sub-bays by funneling the sea water through the tidal channels of Bluefields Bay. Heavy inland flooding from the swollen rivers will further increase water level, which will be blocked from draining immediately to the sea due to Bluefield Bay's restricted entrance. The sediment load should increase due to both the transport of eroded upland material and the resuspension of bay sediments. Upland erosion is heavy under normal conditions; the annual sediment load of the Rio Escondido alone is >10% of that of the Ohio River at

https://doi.org/10.1016/j.yqres.2012.07.003 Published online by Cambridge University Press

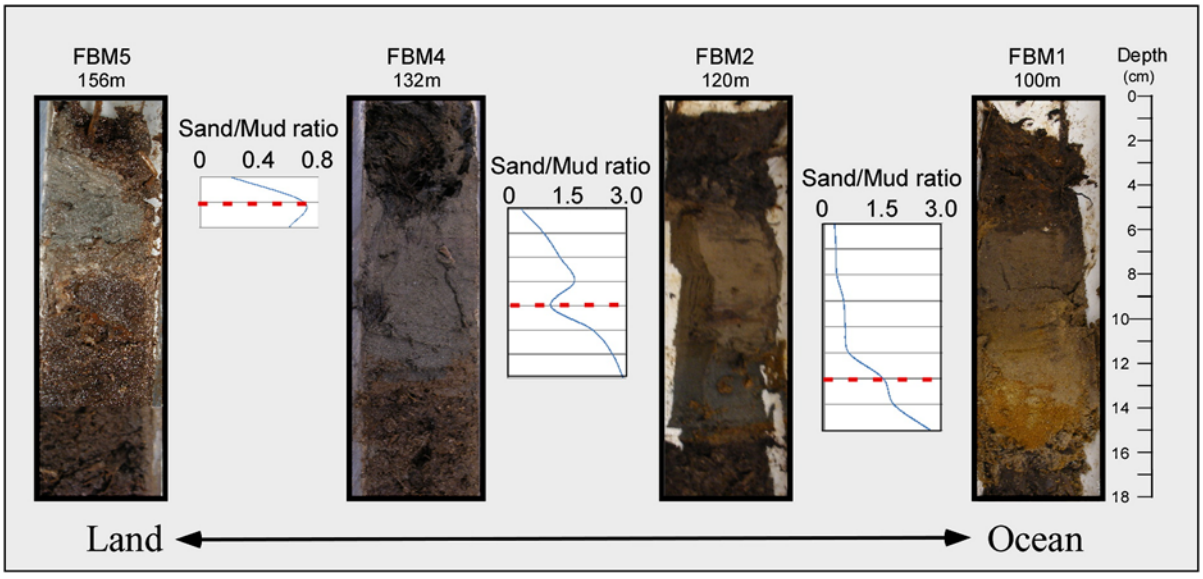

Figure 7. Clastic layer A. Photographs of the layer attributed to Hurricane Joan. The inorganic material thins and fines landward, while fining upward within individual cores. Note the sharp bottom contacts across the transect. Graphs of the mud/sand ratio, calculated at cm resolution are shown in boxes placed at corresponding depths for cores FBM 2, 4, and 5. The dashed red lines mark the boundaries between the lower and upper stratigraphic units.

the confluence with the Mississippi (Heimann et al., 2011). During the extreme precipitation typically accompanying large hurricanes both the sediment load and discharge can be expected to increase dramatically. Given a large enough event, the sediment-laden water will be forced out over the low barriers to the east, with the suspended materials dropping out of the water column. Our coring site in a heavily vegetated depression immediately landward of the beach barrier provides a favorable location for receiving such deposition from the west. The suspended sediments, consisting of resuspended bay material and/or their parent material (eroded upland material), can be expected to resemble the bay bottom sediments (Tables 2 and 3). Similar bimodal sedimentation has been identified as resulting from the traction and suspension loads related to Hurricanes Rita and Ike along the Texas–Louisiana border (Williams, 2009, 2010).

Layer A is overlaid by 5 cm of peat at FBM1 and 2 cm of peat FBM5. Hurricane Joan is the most likely generative event for this layer, being the most recent major hurricane to make landfall in the Bluefields Bay. Layer C probably represents a prehistoric storm as the base of layer in FBM1 is 4 cm above a sample dated to 495 ± 50 ^{14}C yr BP, which calibrates (2σ) to calendar dates ranging from AD 1309 to 1485, before the historical record.

Type 2—back-bay flooding

The sharp bottom contacts and abrupt lithologic changes occurring in compact horizontal bands suggest that these clay layers result from high-energy events. In layers B, D, E and F landward thinning is either missing or greatly reduced, suggesting that deposition occurred principally from the back bay, probably representing hurricanes with smaller storm surges. Pollen data support this view. Currently *Rhizophora* occurs only in the low-energy back-bay area; suggesting that event layers deposited primarily by back-bay flooding should contain higher concentrations of *Rhizophora* pollen than event layers that include a significant overwash component. This seems to be the case as *Rhizophora* concentrations are low in the A and C layers and much higher in two samples from the layer E, and from immediately above layer D. Intervals not associated with clastic layers show generally low *Rhizophora* concentration.

The origins of the indistinct clastic layers at the bottom of Zone 2 in FBM1, 5 (dashed lines, Fig. 5) are more problematic. Although they possibly result from smaller storm events, it is also possible that they represent a transitional phase between Zones 2 and 3, especially the layers in FBM5.

Type 3—evidence of human activity?

The sedimentary layer at 60–100 cm in FBM4, directly above event E, does not occur in the other cores along the transect (Fig. 5). Event E occurs 30–70 cm deeper at FBM4 than in the adjacent cores, suggesting a topographic low, susceptible to rapid filling. This interval is sedimentologically distinct, consisting of a chaotic mixture of organic and clastic materials of widely varying sizes. A woody clump 4 cm in diameter lies discontinuously near the top of the section at 70 cm, while a cleanly cut wood chunk ~2 cm in diameter anchors the bottom at a depth of 92–94 cm, dated stratigraphically to >700 cal yr BP. These two organic pieces are at least an order of magnitude larger than any other material recovered in the transect. The clean and sharp edge of the bottom fragment may suggest cutting by a tool, implying an anthropogenic origin. Conte and Gassiot (2005) have shown extensive human presence with a developed technology as early as 750 BC for the area. We therefore tentatively infer that the anomalous layer in FBM4 is a result of human disturbance at this particular coring site. No evidence of human disturbance was found in other cores along the transect.

Alternative causative agents

Tsunamis offer a possible alternative high-energy source for the deposition of the clastic layers, as tsunami and tropical cyclone deposits cannot always be easily differentiated, despite very different hydrodynamics. Tsunami material is usually transported as suspended load and deposited in sheets, whereas storm sediments are transported as bed load and typically deposited as a wedge much closer to the shore (Morton et al., 2007; Bourgeois, 2009). Because of much larger maximum wave height, tsunami deposits can sometimes be distinguished simply by the size of transported material and the distance and

https://doi.org/10.1016/j.yqres.2012.07.003 Published online by Cambridge University Press

elevations that this material is transported. Other distinguishing sedimentary features of tsunami deposits include the presence of rip-up clasts, poor sorting, and evidence of separate wave trains, often comprised of bidirectional couplets (Nanayama et al., 2000; Goff et al., 2004; Kortekaas and Dawson, 2007; Peters et al., 2007). However, because both tsunami and storm signatures are highly variable and share many common features, they can be confused, particularly if storm surge and tsunami wave heights are similar. At FBM, however, the regional geology makes the occurrence of tsunami deposits unlikely. The tectonic settings present few opportunities for locally generated tsunamis (McCann, 2006), whereas the shallow (maximum water depth<45 m) Nicaraguan rise extends ~250 km offshore (Mills and Hugh, 1974), providing protection against tele-tsunamis. The historical record supports this view. Since 1492 no tsunamis have been recorded for the Caribbean coast of Nicaragua, despite the occurrence of several historical earthquakes that resulted in both land deformation within Nicaragua and tsunamis in neighboring areas (O'Loughlin and Lander, 2003; McCann, 2006; National Geophysical Data Center; http://www.ngdc.noaa.gov/nndc/struts).

Although rain events unrelated to tropical cyclones cannot explain the bottom stratigraphic unit of the type 1 clastic layers, they are a possible causative agent of the type 2 layers. However, it is likely that extreme flooding events at the site are mainly associated with tropical cyclones. Not only does the heaviest rainfall generally occur during tropical cyclones (Riehl, 1979; Gupta, 1988; Scatena and Larsen, 1991; INETER, 1998), but the combination of tropical cyclone-generated precipitation and storm surge is likely to generate much larger floods than non-tropical cyclone-related precipitation events.

With hurricanes being the most likely high-energy event, type 1 layers are posited as representing storms intense enough at the site to deposit a bimodal sedimentary signature that records both storm surge overwash and flooding. The overwash signal (beach/nearshore sand) results from the traction load and is deposited first, while the flooding signal (resuspended bay and newly eroded clay and silt) results from the suspension load delivered from both the ocean and the back bay and is deposited somewhat later. Type 2 layers likely represent flooding from the back bay associated with storms with lower storm surges.

Site sensitivity

The calibration of absolute storm intensity from sedimentary evidence is problematic. Although the water depth associated with storm surge can be calculated based on the grain size of transported material (Woodruff, et al., 2008), no reliable method exists for separating the effects of storm magnitude and proximity, with the result that the sedimentary signatures of a weak storm passing close to the site and a more powerful storm passing at a greater distance can be confused (Liu, 2004). However, site-specific relative differences in storm strength can be inferred on the basis of grain size and layer thickness. In this case, layer A, corresponding to Hurricane Joan, a storm of known intensity and location, can be used to roughly calibrate the local intensities of the other storms. Layer C, very comparable in both thickness and grain size, probably represents a storm of similar intensity, namely a category 4 hurricane making landfall in the immediate vicinity. Given the similarities between the silt/clay in layers B, D, E, and F and the clay layers resulting from the back-bay flooding associated with Hurricane Joan, the storms represented by these layers are probably only slightly weaker than Joan. The E layer is particularly large, from 13 to 15 cm thick in FBM1, 2, and 5. A rough estimate places site sensitivity at major hurricanes (category 3 and above) making landfall in the immediate area. Less distinct clastic layers near the bottom of Zone 2 in FBM1 and Zone 5 possibly represent minor hurricanes.

The FBM record indicates that hurricane landfall frequency has not been constant over the period covered. Five events (A–E) are recorded over the last ~800 yr (700–900 yr with age uncertainty) (Zone 1), giving an average interval of ~160 yr between events (140–180 yr considering uncertainties). During the preceding ~2000 yr (Zone 2) (1800–2100 yr with age uncertainty), a single clear event (F) of comparable magnitude, and one to two lesser events (dashed lines, Fig. 5) occur, yielding a return interval of ~2000 yr (or 600–2100 yr considering uncertainties arising from both age estimates and event counts).

The inferred environment was drastically different during Zone 3, with our coring site located in a marine lagoon, fringed by a dense red mangrove forest (Fig. 6). These conditions should have impeded the transport of hurricane-generated material from both the ocean and back bay, as mangroves can provide significant protection against storm surge by reducing wave energy as much as 50% (Mazda et al., 1997, 2006; Das and Vincent, 2009). Sediment transport can be further restricted due to flow deceleration when encountering the flooded back-bay environment (Horwitz and Wang, 2005). Additionally, the preservation of hurricane-generated deposits is difficult in shallow coastal estuaries due to the resuspension of bottom sediments. For these reasons it is doubtful that hurricanes occurring during this period would have left recognizable signatures in the sedimentary record. No hurricane strikes are recorded for the ~500 yr duration of Zone 4, marking this as a period of reduced tropical cyclone activity.

An alternative explanation is that hurricane activity remained constant while changing sea level affected site sensitivity, with the lower sea levels (hence increased distance to the sea) reducing site sensitivity during the early periods (Liu, 2004). This is unlikely. One distinct (F) and up to two indistinct clastic layers are found in the Zone 2 quiet period in FBM1, 4, and 5, indicating that events were, in fact, being recorded. Palynological evidence indicates that environmental conditions are very comparable for Zones 2 and 4, and that maritime influences from the sea seemed to decrease during Zone 1, as evidenced by increasing frequencies of forest and fresh-brackish wetland taxa such as *Typha* and Cyperaceae. The dated sample at the top of Zone 4 was extracted at a depth of 444 cm when sea level was ~4 m below the present (Toscano and Macintyre, 2003) indicating that the elevation of the site relative to sea level at the time was probably at least as low, and possibly lower, than at present. The evidence therefore supports the view that the lack of clastic intervals in Zone 4 results from lack of hurricane activity and not reduced sensitivity.

This lack of obvious transgression in the last 2800 yr period is probably due to the vast amounts of material being eroded from the central highlands (Mills and Hugh, 1974; Owens and Roberts, 1978; Roberts and Murray, 1983; Marshall, 2007). The existence of open beaches along almost the entire coast, despite microtidal conditions, indicates that coastal elevation is/has been matching the current sea-level rise. This suggests that rising sea level has primarily pushed the nearshore sediments landward and upward, resulting in vertical, rather than horizontal movement of the beaches/barriers.

We recognize that there are inherent uncertainties in using sedimentary evidence to establish long-term strike records, especially the variability in the ability of hurricanes of different intensities to be recorded. However, if boundary conditions remain approximately the same, as we believe they have at FBM during Zones 1, 2, and 4, then large differences in the frequency of strike signatures should correlate with actual changes in strike frequency.

Based on event layers and subject to the uncertainties of dating chronology the tropical cyclone activity pattern can be broadly characterized as:

1. 0–800 cal yr BP—active period (return interval 140–180 yr)
2. 800–2800 cal yr BP—quiet period (return interval 600–2100 yr)
3. 2800–4900 cal yr BP—non-recording, (submerged)
4. 4900–5400 cal BP—quiet period.

The only prehistoric storm previously recorded for the area is an extremely large/unique event recorded from a site 15 km inland that occurred ~3300 cal yr BP during the non-recording period at FBM

https://doi.org/10.1016/j.yqres.2012.07.003 Published online by Cambridge University Press

(Urquhart, 2009). Return intervals differences imply that the regime change from quiet to active increased landfall frequency by a factor of 4–12 at FBM. This is at least as large as the increase associated with the regime change for the northern Gulf of Mexico coast (Liu, 2004).

North Atlantic paleotempestology

A proxy landfall record from Puerto Rico (Donnelly and Woodruff, 2007) identifies active periods at ~5400–3600 cal yr BP, 2500–800 cal yr BP, and the last 250 yr, with quiet periods from 3600 to 2500, and 800 to 250 cal yr BP (Fig. 8b). Proxy records from New England (Scileppi and Donnelly, 2007) display similar temporal patterns, which has led to the argument that hurricane activity levels are controlled by such climatic conditions as ENSO frequency and SST, resulting in synchronous activity regime changes across the North Atlantic (Mann et al., 2009). A contrasting model (Liu and Fearn, 2000; Liu, 2004) suggests that atmospheric steering mechanisms dominate landfall location, and that landfall frequency changes at any location may represent long-term movement of these mechanisms, rather than overall activity levels. Under this scenario, active periods represent the focusing of storm tracks within an area, and are location specific. The forcing mechanism is posited as being the long-term latitudinal position of the main features of the North Atlantic circulation system, principally the Bermuda High and the Intertropical Convergence Zone. During colder periods (increased pole-equator temperature gradient) both features migrate south (Flohn, 1984; Chiang et al., 2003; Chiang and Bitz 2005; Broccoli et al. 2006). Due to the steering control that the Bermuda High exerts over tropical cyclone tracks (Elsner et al., 2000; Elsner, 2003), this movement drives tracks to the south, resulting in increased landfall frequency for southern areas. Active periods are posited as being time-transgressive across the basin and should display a temporally coherent latitudinal drift. This implies that activity regimes in the latitudinal extremes should exhibit anti-phase patterns, with northern areas showing active periods while the southern areas are quiet, and vice-versa. Findings from this study support this time-transgressive model view, displaying a positive relationship with ITCZ latitudinal movement and an inverse relationship with hurricane landfall records from Puerto Rico and the Atlantic coast over the last 2500 yr (Fig. 8).

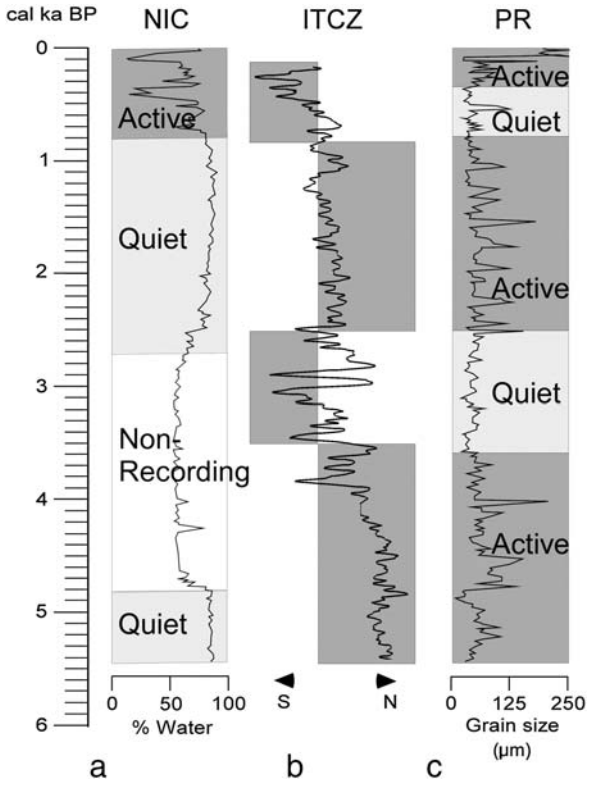

Figure 8. Paleohurricane activity regimes. Diagrams displaying the timing of the active and quiet periods as determined from (a) the FBM transect, and (b) sites along the Atlantic coast of the United States and Puerto Rico. Periods of increased frequency of landfall are shaded in dark gray, reduced landfall in light gray. Curve in (a) is the water percentage from core FBM1; dips to the left indicate hurricane-generated clastic layers. Curve in (c) is the grain size from core LPG4 (Donnelly and Woodruff, 2007); excursions to the right indicate overwash events. Curve in (b) is the bulk titanium content of a core from the Cariaco Basin sediments off of Venezuela, used as a proxy record for the mean latitudinal position of the ITCZ (Haug et al., 2001a, 2001b) (5-point running mean applied). Periods of general northern residency are indicated by shading to the right, while periods of southern residency are shaded to the left. A fairly good agreement can be noted between the latitude of ITCZ residency and hurricane landfall frequency in the proxy records.

Conclusions

A proxy hurricane-landfall record based on overwash events from the ocean to the east and/or flooding from the back bay to the west was developed from a four-core transect extracted from a marsh along the southern Caribbean coast of Nicaragua. The record extends to ~5400 cal yr BP. Calibrations based on the sedimentary signature of Hurricane Joan (1988), which is identified in all transect cores, indicate that the site is recording major hurricanes. Activity levels have not remained constant, with two distinct activity regimes having occurred. The last 800 yr can be characterized as an active period, with an average return period for major hurricanes of ~140–180 yr. This was preceded by a 2000-yr quiet period during which the return period increased to 600–2100 yr. Activity levels cannot be ascertained from ~2800–4900 cal yr BP as environmental conditions rendered the site insensitive to landfall for this period. The period from ~4900–5400 cal yr BP was quiet, with no landfalls recorded. Palynological evidence indicates that active periods are not an effect of reduced site-to-shore distances associated with sea-level rise.

Over the last 2800 yr this pattern is generally anti-phase with the pattern identified from the northern Caribbean and the Atlantic coast of North America, thereby opposing the view that activity regime changes occur simultaneously across the entire North Atlantic basin.

Acknowledgments

This research was supported by grants from the Inter-American Institute for Global Change Research (IAI-CRN2050) and the U.S. National Science Foundation (BCS-0602554). We thank Luo Wang for diatom analysis, Changqing Huang and Saida Nigmatova for pollen analysis of core FBM1, and Brian Atwater for his insightful comments. We also appreciate the help of Gerry Urquhart, Claudia Taleno, and Clifford Herbert in the field and Tom Bianchette in the laboratory.

References

Boucher, D., 1990. Growing back after hurricanes. Bioscience 40, 163–166.
Bourgeois, J., 2009. Geologic effects and records of tsunamis. In: Robinson, A.R., Bernard, E.N. (Eds.), The Sea. Tsunamis, volume 25. Harvard University Press, Boston, pp. 53–91.
Brenes, C.L., Hernandez, A., Ballestero, D., 2007. Flushing time in Perlas Lagoon and Bluefields Bay, Nicaragua. Investigaciones Marinas 35, 89–96.
Broccoli, A.J., Dahl, K.A., Stouffer, R.J., 2006. Response of the ITCZ to Northern Hemisphere cooling. Geophysical Research Letters 33 (Article No. L01702).
Chiang, J.C.H., Bitz, C.M., 2005. Influence of high latitude ice cover on the marine Intertropical Convergence Zone. Climate Dynamics 25, 477–496.
Chiang, J.C.H., Biasutti, M., Battisti, D.S., 2003. Sensitivity of the Atlantic Intertropical Convergence Zone to last glacial maximum boundary conditions. Paleoceanography 18, 1094.
Christie, P., 2000. The people and natural resources of Pearl Lagoon. In: Christie, P., Bradford, D., Garth, R., Gonzalez, B., Hostetler, M., Morales, O., Rigby, R., Simmons, B., Tinkham, E., Vega, G., Vernooy, R., White, N. (Eds.), Taking Care of

What We Have: Participatory Natural Resource Management on the Caribbean Coast of Nicaragua. IDRC Books, Ottawa, pp. 17–46.
Conte, I.C., Gassiot, E., 2005. En el camino de la desigualdad? El litoral de la costa Caribe de Nicaragua entre el 500 cal. ANE y el 450 cal.NE. Revista Atlántica-Mediterránea de Prehistoria y Arqueología Social 7, 109–130.
Das, S., Vincent, J.R., 2009. Mangroves protected villages and reduced death toll during Indian super cyclone. Proceedings of the National Academy of Sciences 106, 7357–7360.
Dean, W.G., 1974. Determination of carbonate and organic matter in calcareous sediments and sedimentary rocks by loss on ignition: comparison with other methods. Journal of Sedimentary Petrology 44, 242–248.
Donnelly, J.P., Webb III, T., 2004. Back-barrier sedimentary records of intense hurricane landfalls in the northeastern United States. In: Murnane, R.J., Liu, K.-b. (Eds.), Hurricanes and Typhoons: Past, Present and Future. Columbia University Press, New York, pp. 58–95.
Donnelly, J.P., Woodruff, J., 2007. Intense hurricane activity over the past 5000 years controlled by El Nino and the West African Monsoon. Nature 44, 465–468.
Elsner, J.B., 2003. Tracking hurricanes. Bulletin of the American Meteorological Society 84, 353–356.
Elsner, J.B., Liu, K.-B., Kocher, B., 2000. Spatial variations in major U.S. hurricane activity: statistics and a physical mechanism. Journal of Climate 13, 2293–2305.
Faegri, K., Iverson, J., 1989. Textbook of Pollen Analysis. John Wiley & Sons, Chichester.
Flohn, H., 1984. Ice-free Arctic and glaciated Antarctic. In: Flohn, H., Fantechi, R. (Eds.), The Climate of Europe: Past, Present and Future. D. Reidel Publishing Company, Dordrecht, pp. 248–268.
Gerrish, H.P., 1989. Preliminary Report Hurricane Joan 10–23 October 1988. http://www.nhc.noaa.gov/archive/storm_wallets/atlantic/atl1988-prelim/joan/prelim01.gif Accessed Dec. 21, 2011.
Goff, J., McFadgen, B.G., Chague-Goff, C., 2004. Sedimentary differences between the 2002 Easter storm and the 15th-century Okoropunga tsunami, southeastern North Island, New Zealand. Marine Geology 204, 235–250.
Gupta, A., 1988. Large floods as geomorphic events in the humid tropics. In: Baker, V.R., Kochel, R.C., Patton, P.C. (Eds.), Flood Geomorphology. John Wiley and Sons, New York, pp. 310–315.
Haug, G.H., Hughen, K.A., Sigman, D.M., Peterson, L.C., Rohl, U., 2001a. Southward migration of the intertropical convergence zone through the Holocene. Science 293, 1304–1308.
Haug, G.H., Hughen, K.A., Sigman, D.M., Peterson, L.C., Rohl, U., 2001b. Cariaco Basin Trace Metal Data. IGBP PAGES/World Data Center A for Paleoclimatology. Data Contribution Series #2001-071. NOAA/NGDC Paleoclimatology Program, Boulder, CO, USA.
Heimann, D.C., Sprague, L.A., Blevins, D.W., 2011. Trends in suspended-sediment loads and concentrations in the Mississippi River Basin, 1950–2009. U.S. Geological Survey Scientific Investigations Report 2011-5200.
Horwitz, M., Wang, P., 2005. Sedimentological characteristics and internal architecture of two overwash fans from Hurricanes Ivan and Jeanne. Gulf Coast Association of Geological Societies Transactions 55, 342–352.
INETER, 1998. Mitch vs. las lluvias provocadas durante el period de affectation de otros huracanes. Las Lluvias del Siglo en Nicaragua. Instituto Nicarauense de Estudio Territoriales, Managua, Nicaragua, pp. 43–45.
Kortekaas, S., Dawson, A.G., 2007. Distinguishing tsunami and storm deposits: an example from Martinhal SW Portugal. Sedimentary Geology 200, 208–211.
Lawrence, M.B., Gross, J.M., 1989. Annual summaries Atlantic hurricane season of 1988. Monthly Weather Reviews 117, 2248–2259.
Liu, K.-b., 2004. Paleotemstology: principles, methods and examples from Gulf coast lake sediments. In: Murnane, R.J., Liu, K.-b. (Eds.), Hurricanes and Typhoons: Past, Present and Future. Columbia University Press, New York, pp. 13–57.
Liu, K.-b., Fearn, M.L., 1993. Lake-sediment record of late Holocene hurricane activities from coastal Alabama. Geology 21, 793–796.
Liu, K.-b., Fearn, M.L., 2000. Reconstruction of prehistoric landfall frequencies of catastrophic hurricanes in northwestern Florida from lake sediment records. Quaternary Research 54, 238–245.
Mann, M.E., Woodruff, J.D., Donnelly, J.P., Zhang, Z., 2009. Atlantic hurricanes and climate over the past 1,500 years. Nature 460, 880–883.
Marshall, J.S., 2007. Coastal morphology and coastal reefs. In: Bundschuh, J., Alvarado, G.E. (Eds.), Central America Geology Resource Hazards, vol. 1. Taylor and Francis, London, pp. 185–200.
Mazda, Y., Magi, M., Kogo, M., Hong, P.N., 1997. Mangroves as coastal protection from waves in the Tong King delta, Vietnam. Mangroves and Salt Marshes 1, 127–135.
Mazda, Y., Michimasa, M., Ikeda, Y., Kurokawa, T., Tetsumi, A., 2006. Wave reduction in a mangrove forest dominated by *Sonneratia* sp. Wetlands Ecology and Management 14, 365–378.
McCann, W.R., 2006. Estimating the threat of tsunamigenic earthquakes and earthquake induced-landslide tsunamis in the Caribbean. In: Mercado-Irizarry, A., Liu, P. (Eds.), Caribbean Tsunami Hazard. World Scientific Publishing Company, New Jersey, pp. 43–65.
McCloskey, T.A., Keller, G., 2009. 5000 year sedimentary record of hurricane strikes on the central coast of Belize. Quaternary International 195, 53–68.
McCloskey, T.A., Knowles, J.T., 2009. Migration of the tropical cyclone zone through the Holocene. In: Elsner, J.B., Jagger, T.H. (Eds.), Hurricanes and Climate Change. Springer, New York, pp. 169–188.
Mills, R.A., Hugh, K.E., 1974. Reconnaissance group map of Mosquitia region, Honduras and Nicaragua Caribbean coast. The Association of American Petroleum Geologist Bulletin 58, 189–207.
Morton, R.A., Gelfenbaum, G., Jaffe, B.E., 2007. Physical criteria for distinguishing sandy tsunami and storm deposits using modern examples. Sedimentary Geology 200, 184–207.
Nanayama, F., Shigeno, K., Satake, K., Shimokawa, K., Koitabashi, S., Miyasaka, S., Ishii, M., 2000. Sedimentary differences between the 1993 Hokkaido–Nansei–Oki tsunami and the 1959 Miyakojima typhoon at Taisei, southwestern Hokkaido, northern Japan. Sedimentary Geology 135, 255–264.
O'Loughlin, K.F., Lander, J.F., 2003. Caribbean Tsunamis: A 500 Year History, 1498–1998. Kluwer Academic Publishers, Norwell, MA.
Owens, E.H., Roberts, H.H., 1978. Variations of wave-energy levels and coastal sedimentation, eastern Nicaragua. Proceedings of the 16th Conference on Coastal Engineering, pp. 119–1214.
Parsons, J.J., 1955. The Miskito pine savanna of Nicaragua and Honduras. Annals of the Association of American Geographers 45, 36–63.
Peters, R., Jaffe, B.E., Gelfenbaum, G., 2007. Distribution and sedimentary characteristics of tsunami deposits along the Cascadia margin of western North America. Sedimentary Geology 200, 372–386.
Reimer, P.J., Baillie, M.G.L., Bard, E., Bayliss, A., Beck, J.W., Blackwell, P.G., Bronk Ramsey, C., Buck, C.E., Burr, G.S., Edwards, R.L., Friedrich, M., Grootes, P.M., Guilderson, T.P., Hajdas, I., Heaton, T.J., Hogg, A.G., Hughen, K.A., Kaiser, K.F., Kromer, B., McCormac, F.G., Manning, S.W., Reimer, R.W., Richards, D.A., Southon, J.R., Talamo, S., Turney, C.S.M., van der Plicht, J., Weyhenmeyer, C.E., 2009. IntCal09 and Marine09 radiocarbon age calibration curves, 0–50,000 years cal BP. Radiocarbon 51, 1111–1150.
Riehl, H., 1979. Climate and Weather in the Tropics. Academic Press, New York.
Roberts, H.H., Murray, S.P., 1983. Controls on reef development and the terrigenous–carbonate interface on a shallow shelf, Nicaragua (Central America). Coral Reefs 2, 71–80.
Scatena, F.N., Larsen, M.C., 1991. Physical aspects of Hurricane Hugo in Puerto Rico. Biotropica 23, 317–323.
Scileppi, E., Donnelly, J.P., 2007. Sedimentary evidence of hurricane strikes in western Long Island, New York. Geochemistry, Geophysics, Geosystems 8 (doi:Q06011Artn q06011).
Scott, D.B., Collins, E.S., Gayes, P.T., Wright, E., 2003. Records of prehistoric hurricanes on the South Carolina coast based on micropaleontological and sedimentological evidence, with comparison to other Atlantic Coast records. Geological Society of America Bulletin 115, 1027–1039.
Toscano, M.A., Macintyre, I.G., 2003. Corrected western Atlantic sea-level curve for the last 11,000 years based on calibrated C-14 dates from *Acropora palmate* framework and intertidal mangrove peat. Coral Reefs 22, 257–270.
Urquhart, G.R., 2009. Paleoecological record of hurricane disturbance and forest regeneration in Nicaragua. Quaternary International 195, 88–97.
Vandermeer, J.H., Granzow de la Cerda, I., Boucher, D., Perfecto, I., Ruiz, J., 2000. Hurricane disturbance and tropical tree species diversity. Science 290, 788–790.
Wallace, D.R., 1997. Central American landscapes. In: Coates, A.G. (Ed.), Central America: A Natural and Cultural History. Yale University Press, New Haven, pp. 72–96.
Williams, H.F.L., 2009. Stratigraphy, sedimentology, and microfossil content of Hurricane Rita storm surge deposits in southwest Louisiana. Journal of Coastal Research 25, 1041–1051.
Williams, H.F.L., 2010. Storm surge deposition by Hurricane Ike on the McFadden National Wildlife Refuge, Texas: implications for paleotempestology studies. Journal of Foraminiferal Research 40, 510–519.
Woodruff, J.D., Donnelly, J.P., Mohrig, D., Geyer, W.R., 2008. Reconstructing relative flooding intensities responsible for hurricane-induced deposits from Laguna Playa Grande, Puerto Rico. Geology 36, 391–394.